Journal of Materials Chemistry A

Accepted Manuscript

ROYAL SOCIETY OF CHEMISTRY

www.rsc.org/materialsA

Journal Name

ARTICLE

Construction of hierarchical $ZnCo_2O_4@Ni_xCo_{2x}(OH)_{6x}$ core/shell nanowire arrays for high-performance supercapacitors

Received 00th January 20xx,
Accepted 00th January 20xx

DOI: 10.1039/x0xx00000x

www.rsc.org/

Wenbin Fu,[a] Yaling Wang,[a] Weihua Han,[a,*] Zemin Zhang,[a] Heming Zha,[b] and Erqing Xie[a,*]

Rational design and synthesis of core/shell nanostructures as binder-free electrodes has been believed to be an effective strategy to improve the electrochemical performance of supercapacitors. In this work, hierarchical $ZnCo_2O_4@Ni_xCo_{2x}(OH)_{6x}$ core/shell nanowire arrays (NWAs) have been successfully constructed by electrodepositing $Ni_xCo_{2x}(OH)_{6x}$ nanosheets onto hydrothermally grown $ZnCo_2O_4$ nanowires and investigated as a battery-type electrode for hybrid supercapacitors. Taking advantage of the hierarchical core/shell structures and the synergetic effect between $ZnCo_2O_4$ nanowires and $Ni_xCo_{2x}(OH)_{6x}$ nanosheets, the optimised core/shell electrode exhibits remarkable electrochemical performance with a high areal capacity (419.1 μAh cm^{-2}), good rate capability and cycling stability. Moreover, the assembled $ZnCo_2O_4@Ni_xCo_{2x}(OH)_{6x}$//activated carbon (AC) hybrid device can be reversibly cycled in a large potential range of 0−1.7 V and deliver a maxium energy density of 26.2 Wh kg^{-1} at 511.8 W kg^{-1}. Our findings indicate that the hierarchical $ZnCo_2O_4@Ni_xCo_{2x}(OH)_{6x}$ core/shell NWAs has great potential for applications in energy storage devices.

1. Introduction

With the increasing desire for the utilization of renewable and clean energy sources, energy storage has become one of the biggest challenges in 21st century.[1-3] Supercapacitors have attracted significant attention as one type of efficient energy storage devices due to their high power density, fast charge-discharge rate, long cycle life and safe operation.[4] Based on the charge storage mechanism, supercapacitors are generally divided into electrical double layer capacitors (EDLCs) and pseudocapacitors.[5] However, as for the two categories, their energy density is still too low, which impedes their practical applications.[6,7] Hybrid supercapacitors consisting of an EDLC-type (or pseudocapacitive) electrode and a battery-type electrode can achieve higher energy density than conventional capacitors and higher power density than batteries.[8-10] Thus, numerous efforts have been dedicated to develop battery-type materials that undergo faradic reactions, including metal oxides, hydroxides and sulfides.[11-14] Among them, $Ni(OH)_2$ and $Co(OH)_2$ have been widely studied as electrode materials for hybrid supercapacitor due to their natural abundance and low cost.[15,16] $Ni(OH)_2$ has a high theoretical specific capacity but suffers from its instinct poor conductivity which restricts its rate capability.[17,18] While $Co(OH)_2$ can exhibit higher conductivity than $Ni(OH)_2$. More interestingly, Ni-Co hydroxide is found to integrate the advantages of $Ni(OH)_2$ and $Co(OH)_2$ and exhibit higher rate capability.[19-21] However, the rate capability and cycling performance are still unsatisfactory.

Recently, $ZnCo_2O_4$ is particularly concerned for energy storage applications owning to its superior electrochemical properties.[22-24] By partially replacing Co^{2+} by Zn^{2+}, $ZnCo_2O_4$ can exhibit higher conductivity and better electrochemical activity than pure Co_3O_4.[25-27] Thus far, various types of $ZnCo_2O_4$ nanostructures have been prepared as battery-type electrode materials for hybrid supercapacitors.[27-31] Although some progress has been made for $ZnCo_2O_4$, the areal (specific) capacity is still limited and need to be further improved to meet the demand for high-performance devices.

To improve the electrochemical performance, constructing core/shell hybrid nanostructures on conductive substrates as binder-free electrodes has been considered as one of effective strategies.[32-34] Generally, the core materials are one-dimensional (1D) nanowires (or nanorods/nanotubes), which would create stable and efficient pathways for electron transport. The shell materials are promising as two-dimensional (2D) nanosheets (or nanoflakes), which can significantly increase the surface area and provide more electrochemical active sites.[33,35,36] As a result, such core/shell structures can shorten the distance for electrolyte ion diffusion and open up more efficient pathways for electron transport.[37,38] Given these merits, considerable efforts have been devoted to developing various core/shell configurations (e.g., H-CoO_x@$Ni(OH)_2$ NWAs,[39] $NiCo_2O_4$@MnO_2 NWAs,[40] $NiCo_2S_4$/$Co_xNi_{1-x}(OH)_2$ nanotube arrays[41]) for supercapacitors and achieved improved electrochemical performance.

Herein, we demonstrate a facile strategy for the construction of hierarchical $ZnCo_2O_4@Ni_xCo_{2x}(OH)_{6x}$ core/shell NWAs, including hydrothermal synthesis of $ZnCo_2O_4$ NWAs and electrodeposition of $Ni_xCo_{2x}(OH)_{6x}$ nanosheets (the mixture of

[a] School of Physical Science and Technology, Lanzhou University; [b] Cuiying Honors College, Lanzhou University, Lanzhou, 730000, China. Email: hanwh@lzu.edu.cn (Weihua Han); xieeq@lzu.edu.cn (Erqing Xie). Tel.: +86 931 8912616

Electronic Supplementary Information (ESI) available: [XRD patterns, additional results of electrochemical tests]. See DOI: 10.1039/x0xx00000x

$Ni(OH)_2$ and $Co(OH)_2$ with a molar ratio of 1/2). Benefiting from the rational construction, the core/shell nanostructures can show good conductivity, large surface area and sufficient active sites, which are favorable for the electrolyte ion diffusion and provide more efficient pathways for electron transport. This hybrid electrode based on the core/shell nanostructures exhibits a high areal capacity of 419.1 μAh cm^{-2} at the current density of 5 mA cm^{-2}, good rate capability (253.4 μAh cm^{-2} at 50 mA cm^{-2}) and cycling stability (81.4% of capacity retention after 2000 cycles at 20 mA cm^{-2}). A hybrid supercapacitor has been fabricated by using the $ZnCo_2O_4$@$Ni_xCo_{2x}(OH)_{6x}$ NWAs as the positive electrode and activated carbon (AC) as the negative electrode. The hybrid device can present a high energy density of 26.2 Wh kg^{-1} at a power density of 511.8 W kg^{-1}. This work would provide an effective strategy to construct core/shell hybrid nanostructures for energy storage devices.

2. Experimental

In this work, the effective strategy for constructing hierarchical $ZnCo_2O_4$@$Ni_xCo_{2x}(OH)_{6x}$ core/shell NWAs is schematically illustrated in Fig. 1. Firstly, Zn-Co precursors were vertically grown on Ni foam by a hydrothermal reaction and $ZnCo_2O_4$ NWAs were formed after a post annealing treatment. Then $Ni_xCo_{2x}(OH)_{6x}$ nanosheets were electrodeposited onto the $ZnCo_2O_4$ NWAs, resulting in the core/shell nanostructures.

All the reagents were of analytical grade and used without further purification. Ni foam (100 pores per inch, ~ 38 mg cm^{-2}, ~ 1.5 mm thick) was purchased from Lyrun New Material Co. Ltd. (Changsha, China).

2.1 Synthesis of $ZnCo_2O_4$ NWAs

Firstly, Ni foam was ultrasonically cleaned with acetone, 3 M HCl solution, deionized water and ethanol for 15 min each to remove the impurities and oxide layer. In a typical process, 0.5 mmol $Zn(NO_3)_2 \cdot 6H_2O$, 1 mmol $Co(NO_3)_2 \cdot 6H_2O$, 1 mmol NH_4F and 2.5 mmol urea were dissolved in 35 mL deionized water and magnetically stirred for about 15 min until it formed a homogeneous solution. The obtained solution was transferred into a 50 mL Teflon-lined stainless-steel autoclave and a piece of cleaned Ni foam (2.5 cm × 4.0 cm) was vertically placed into the solution against the bottom of the autoclave. Then the autoclave with the solution was maintained at 120 °C for 5 h. After cooling down to room temperature naturally, the products were taken out and rinsed with deionized water and ethanol several times. The precursors were dried at 60 °C for 10 h and finally annealed in a quartz tube at 400 °C for 2 h. The mass loading of $ZnCo_2O_4$ NWAs on Ni foam is ~ 1.8 mg cm^{-2}.

2.2 Electrodeposition of $Ni_xCo_{2x}(OH)_{6x}$ nanosheets

The $Ni_xCo_{2x}(OH)_{6x}$ nanosheets were deposited on $ZnCo_2O_4$ NWAs using an electrochemical workstation (CS310, Wuhan Corrtest Instruments Co. Ltd., China) with a three-electrode configuration. In this procedure, the as-prepared $ZnCo_2O_4$ NWAs were used as the working electrode, a saturated calomel electrode (SCE) as the reference electrode, and a platinum plate as the counter electrode, respectively. The electrodeposition was carried out in 50 mL aqueous electrolyte consisting of 4 mM $Ni(NO_3)_2$ and 8 mM $Co(NO_3)_2$ using the potential static technique at -1.0 V for 10 min at room temperature. The obtained products were carefully rinsed with deionized water and dried in a vacuum oven at 60 °C for 12 h. The final mass loading of $ZnCo_2O_4$@$Ni_xCo_{2x}(OH)_{6x}$ NWAs on Ni foam is ~ 2.5 mg cm^{-2}. For comparison, the $Ni_xCo_{2x}(OH)_{6x}$ nanosheets were deposited on Ni foam for 14 min to obtain the same mass loading (~ 0.7 mg cm^{-2}) with that on $ZnCo_2O_4$ NWAs.

2.3 Material characterization

The morphology and microstructure were characterized with scanning electron microscopy (SEM, Tescan MIRA 3 XMU) and transmission electron microscopy (TEM, FEI Tecnai F30) equipped with energy dispersive x-ray spectroscopy (EDX, AMETEK, USA). The phase structure was identified by X-ray diffraction (XRD, Philips X'pert pro) with Cu Kα radiation (0.154056 nm) and the chemical composition was examined with an X-ray photoelectron spectroscopy (XPS, PHI-5702), using Mg Kα X-ray (hν = 1253.6 eV) as the excitation source. The loaded mass of the active materials was measured using a microbalance (Mettler, XS105DU).

2.4 Electrochemical measurements

All the electrochemical measurements were carried out using the same electrochemical workstation (CS310, Wuhan Corrtest Instruments Co. Ltd., China) in 2 M KOH aqueous electrolyte at room temperature. The samples were investigated in a three-electrode configuration with the nanostructures grown on Ni foam (1.0 cm × 1.0 cm) as the working electrodes, a SCE as the reference electrode and a platinum plate as the counter electrode. Cyclic voltammetry (CV) and galvanostatic charge-discharge (GCD) measurements were carried out to evaluate the electrochemical performance of the electrodes. Electrochemical

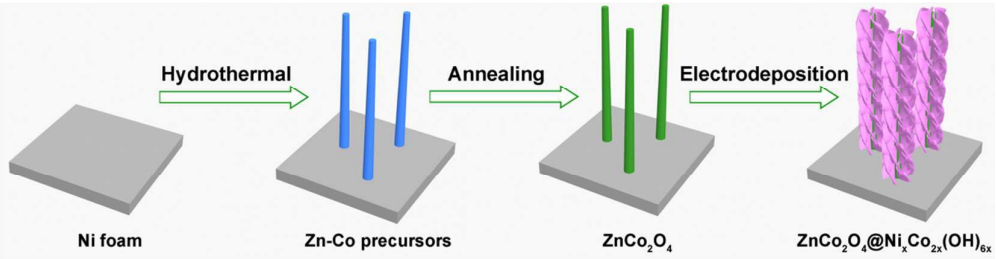

Fig. 1 Schematic illustration of the construction process of hierarchical $ZnCo_2O_4$@$Ni_xCo_{2x}(OH)_{6x}$ core/shell NWAs on Ni foam.

impedance spectroscopy (EIS) analysis was recorded with a superimposed 5 mV sinusoidal voltage in the frequency range of 100 kHz−0.01 Hz.

2.5 Fabrication of a hybrid supercapacitor

The hybrid supercapacitor was fabricated by using the $ZnCo_2O_4$@$Ni_xCo_{2x}(OH)_{6x}$ NWAs as the positive electrode, AC as the negative electrode, cellulose paper as the separator and 2 M KOH as the aqueous electrolyte. The AC electrode was prepared by a typical procedure.[18] In brief, AC, acetylene black and polyvinylidene fluoride (PVDF) with a mass ratio of 80:10:10 were mixed in N-methylpyrrolidinone (NMP) to obtain homogeneous slurry. Then the slurry was coated onto a piece of cleaned Ni foam (1.0 cm × 1.0 cm) with a blade and dried under vacuum at 80 °C for 12 hours. Two-electrode tests were conducted to evaluate the electrochemical performance of the hybrid device.

The areal capacity (Q_a) of the electrodes can be calculated from the discharge curves according to the following equation:

$$Q_a = (I \times \Delta t)/A \quad (1)$$

where I is the current density, Δt is the discharge time and A is the area of the electrodes.

Energy density (E) and power density (P) of the device can be evaluated according to the following equations:

$$E = \int I \times V(t) dt \quad (2)$$

$$P = E/\Delta t \quad (3)$$

where I is the current density, $V(t)$ is the cell voltage, dt is the time differential and Δt is the discharge time.

3. Results and discussion

Fig. 2a shows SEM images of $ZnCo_2O_4$ NWAs on Ni foam. It can be seen that numerous needle-like $ZnCo_2O_4$ nanowires were vertically grown on the surface of Ni foam framework, leading to a stable and porous three-dimensional (3D) network with large surface area and appropriate space (insert of Fig. 2a). A magnified SEM image (Fig. 2b) indicates that the $ZnCo_2O_4$ nanowires have an average diameter of 80 nm and a length of 4–6 μm. After electrodeposition, the slim $ZnCo_2O_4$ nanowires were uniformly decorated with interconnected $Ni_xCo_{2x}(OH)_{6x}$ nanosheets, forming unique forest-like core/shell arrays (Fig. 2c). Obviously, the nanosheets are ultrathin and wrinkled (Fig. 2d), which further increases the surface area of the electrode and provides more active sites for the redox reactions.

TEM was conducted to further detail the microstructures of the samples. As presented in Fig. 3a, the $ZnCo_2O_4$ nanowire has a diameter of ~ 80 nm, similar with the SEM observations. The nanowire is composed of many interconnected nanoparticles, which may be attributed to the gas release during annealing. The high-resolution TEM (HRTEM) image (Fig. 3b) indicates a

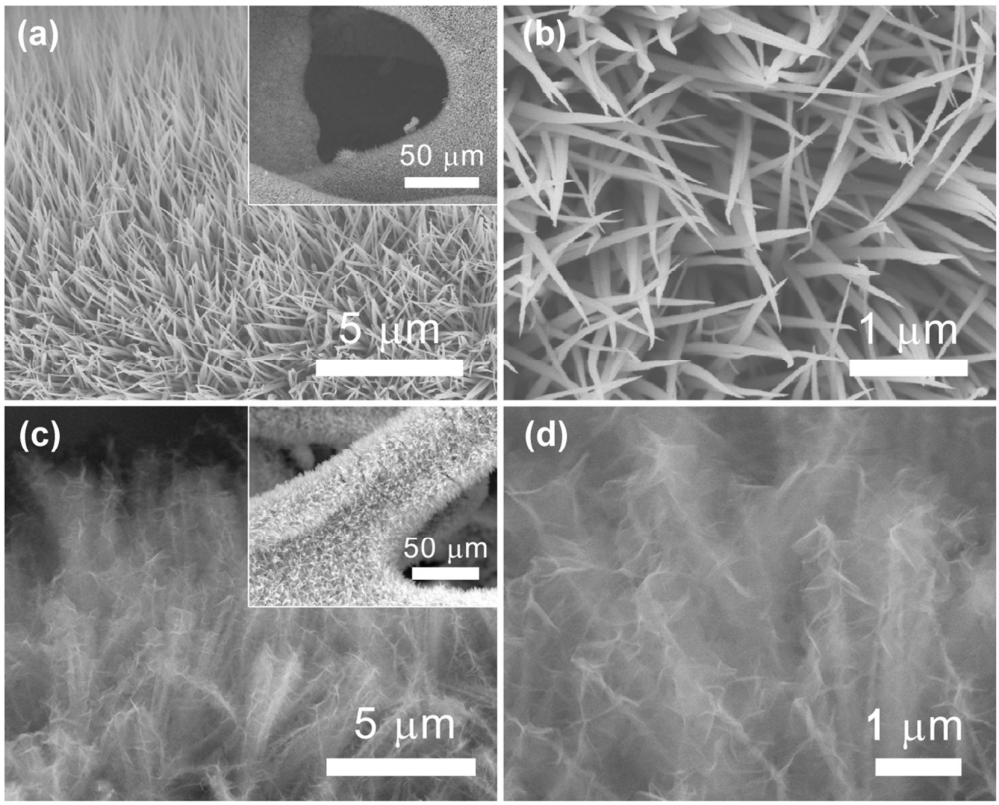

Fig. 2 SEM images of $ZnCo_2O_4$ NWAs (a and b) and $ZnCo_2O_4$@$Ni_xCo_{2x}(OH)_{6x}$ NWAs (c and d) on Ni foam at different magnifications.

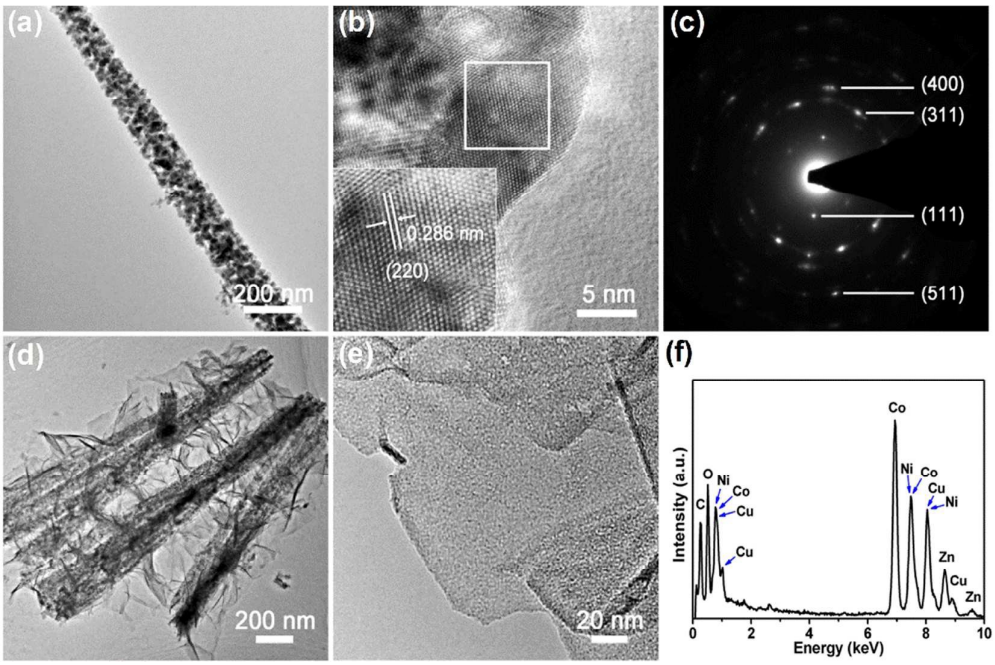

Fig. 3 TEM image (a), HRTEM image (b) and SAED pattern (c) of the $ZnCo_2O_4$ nanowire. TEM images (d and e) and EDX spectrum (f) of the $ZnCo_2O_4$@$Ni_xCo_{2x}(OH)_{6x}$ NWAs.

good crystallinity of the $ZnCo_2O_4$ nanowire. The inset of Fig.3b is a magnified image taken from the highlighted region by a white square. It demonstrates that the spacing of the lattice plane is about 0.286 nm, corresponding to the distance of the (220) planes of spinel $ZnCo_2O_4$ (JCPDS card No. 23-1390). Fig. 3c shows a selected area of electron diffraction (SAED) pattern of the $ZnCo_2O_4$ nanowire. And the reflection rings correspond to (111), (311), (400) and (511) planes of spinel $ZnCo_2O_4$, which further confirms its crystal structure. As shown in Fig. 3d, the $ZnCo_2O_4$ nanowires were uniformly coated with interconnected nanosheets after electrodeposition. These nanosheets are ultrathin and consisted of numerous pores (several nanometers in size) throughout the surface (Fig. 3e), as previously reported.[42,43] It is well noted that the hierarchical core/shell nanostructures would not only create an open and conductive network for electrolyte diffusion and electron transport, but also provide large surface area and sufficient active sites for redox reactions. In addition, the EDX spectrum (Fig. 3f.) of the $ZnCo_2O_4$@$Ni_xCo_{2x}(OH)_{6x}$ NWAs demonstrates that the core/shell hybrid structures are mainly composed of Co, Ni, Zn and O elements, except for Cu and C signals from the carbon supported Cu grid.

XRD analysis was performed to identify the phase structures of the samples. To avoid the influence from Ni foam (Fig. S1a and S2†), the nanostructures were scratched from Ni foam. The XRD patterns of the obtained $ZnCo_2O_4$, $Ni_xCo_{2x}(OH)_{6x}$ and $ZnCo_2O_4$@$Ni_xCo_{2x}(OH)_{6x}$ nanostructures are displayed in Fig. 4. The strong peaks at 31.2°, 36.8°, 44.8°, 59.3° and 65.1° can respectively correspond to the (220), (311), (400), (511) and (440) planes of the spinel $ZnCo_2O_4$. The diffraction peaks for the $Ni_xCo_{2x}(OH)_{6x}$ nanosheets are weak and broad, indicating the low crystallinity, which can match with those of α-$Ni(OH)_2$ (JCPDS card No. 38-0715) and $Co(OH)_2$ (JCPDS card No. 30-0443). Besides, the Ni-Co hydroxides can convert into $NiCo_2O_4$ (JCPDS card No. 30-0443) after annealing at 400 °C for 2h (Fig. S1b†), indicating that the molar ratio of Ni and Co in the Ni-Co hydroxides is 1: 2.

X-ray photoelectron spectroscopy (XPS) analysis was carried out to further confirm the chemical composition. A survey XPS spectrum of the $ZnCo_2O_4$@$Ni_xCo_{2x}(OH)_{6x}$ NWAs (Fig. 5a) reveals the presence of Zn, Ni, Co, O and C elements, which is in agreement with the EDX results. The high-resolution XPS spectrum of Zn 2p (Fig. 5b) demonstrates that the two major peaks at 1044.9 eV and 1021.9 eV are respectively ascribed to Zn $2p_{3/2}$ and Zn $2p_{1/2}$ of the Zn^{2+} oxidation state in the $ZnCo_2O_4$ nanowires.[44] As shown in Fig. 5c, two peaks centered at 873.7 eV and 856.1 eV are corresponding to Ni $2p_{1/2}$ and Ni $2p_{3/2}$, indicating the Ni^{2+} oxidation state in Ni-Co hydroxides.[20] Two

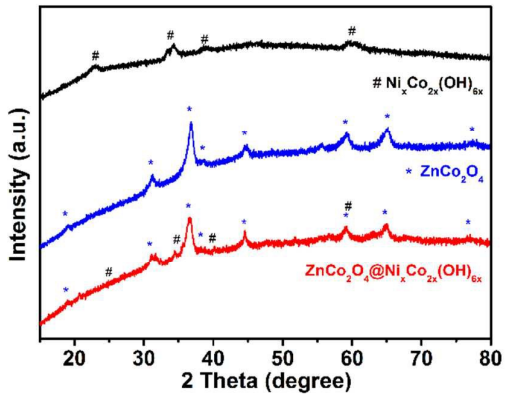

Fig. 4 XRD patterns of the $ZnCo_2O_4$, $Ni_xCo_{2x}(OH)_{6x}$ and $ZnCo_2O_4$@$Ni_xCo_{2x}(OH)_{6x}$ nanostructures scratched from Ni foam.

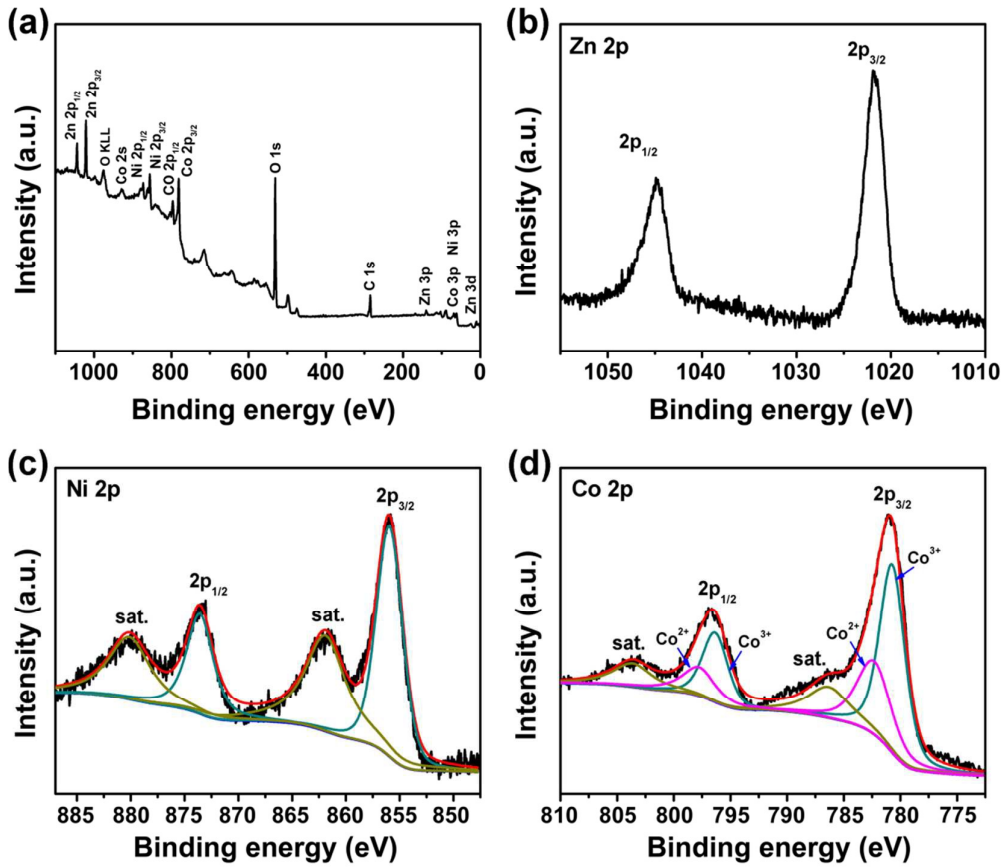

Fig. 5 XPS spectra for the $ZnCo_2O_4$@$Ni_xCo_{2x}(OH)_{6x}$ core/shell NWAs: survey spectrum (a) and high-resolution spectra of Zn 2p (b), Ni 2p (c) and Co 2p (d).

kinds of Co species (Co^{2+} and Co^{3+}) were detected in the Co 2p spectra (Fig. 5d). The strong peaks at 796.5 eV for Co $2p_{1/2}$ and 780.9 eV for Co $2p_{3/2}$ reveal the Co^{3+} oxidation state in $ZnCo_2O_4$ phase.[45] The peaks at 798.2 eV and 782.5 eV are ascribed to the presence of the Co^{2+} oxidation state in the $Ni_xCo_{2x}(OH)_{6x}$ nanosheets.[46] The O 1s spectra (Fig. S3†) reveal the presence of metal-oxygen bands in $ZnCo_2O_4$ nanowire and metal-hydrogen-oxygen bands in $Ni_xCo_{2x}(OH)_{6x}$ nanosheet.[20,47]

Three-electrode measurements were conducted to investigate the electrochemical performance of electrodes. Fig 6a shows a comparison of cyclic voltammetry (CV) curves for the prepared electrodes within the potential window of -0.1–0.5 V at the same scan rate of 10 mV s^{-1}. It can be seen that all the CV curves have obvious redox peaks, revealing the faradic nature of the battery-type electrodes. For the $ZnCo_2O_4$ electrode, a pair of strong redox peaks are owning to the faradaic redox reactions assigned to the $Co(OH)_2$/CoOOH redox couple prior to the onset of oxygen evolution.[27,29] For the $Ni_xCo_{2x}(OH)_{6x}$ electrode, the redox peaks are attributed to the Faradaic reactions of the Ni-Co hydroxides with the electrolyte ions. In contrast, the CV curve of the $ZnCo_2O_4$@$Ni_xCo_{2x}(OH)_{6x}$ electrode with stronger redox peaks indicates a combinative faradic characteristics of the two materials. The redox reactions in the alkaline electrolyte for the core/shell hybrid electrode can be described as the following equations:[43,48]

$$Co_2O_4^{2-} + 2H_2O + OH^- \leftrightarrow 2CoOOH + e^- \quad (4)$$

$$Co(OH)_2 + OH^- \leftrightarrow CoOOH + H_2O + e^- \quad (5)$$

$$Ni(OH)_2 + OH^- \leftrightarrow NiOOH + H_2O + e^- \quad (6)$$

$$CoOOH + OH^- \leftrightarrow CoO_2 + H_2O + e^- \quad (7)$$

The hybrid electrode shows a significant larger integrated CV area which implies its higher capacity. The integrated area for the cleaned Ni foam is limited when compared with that of the hybrid electrode, suggesting the capacity contribution from the cleaned Ni foam is negligible (Fig. S4†). Moreover, the CV curves of the $ZnCo_2O_4$@$Ni_xCo_{2x}(OH)_{6x}$ electrode at the scan rates of 5–50 mV s^{-1} are shown in Fig. 6b. With increasing the scan rate, the position of the cathodic peak gradually shifts towards a more cathodic position and the anode peak towards a more anodic direction, implying a good rate capability of the hybrid electrode.

Fig. 6c shows the galvanostatic charge-discharge (GCD) curves of the $ZnCo_2O_4$@$Ni_xCo_{2x}(OH)_{6x}$ electrode at the current densities ranging from 5 to 50 mA cm^{-2} within the potential window of 0–0.45 V. Obviously, the potential plateaus between

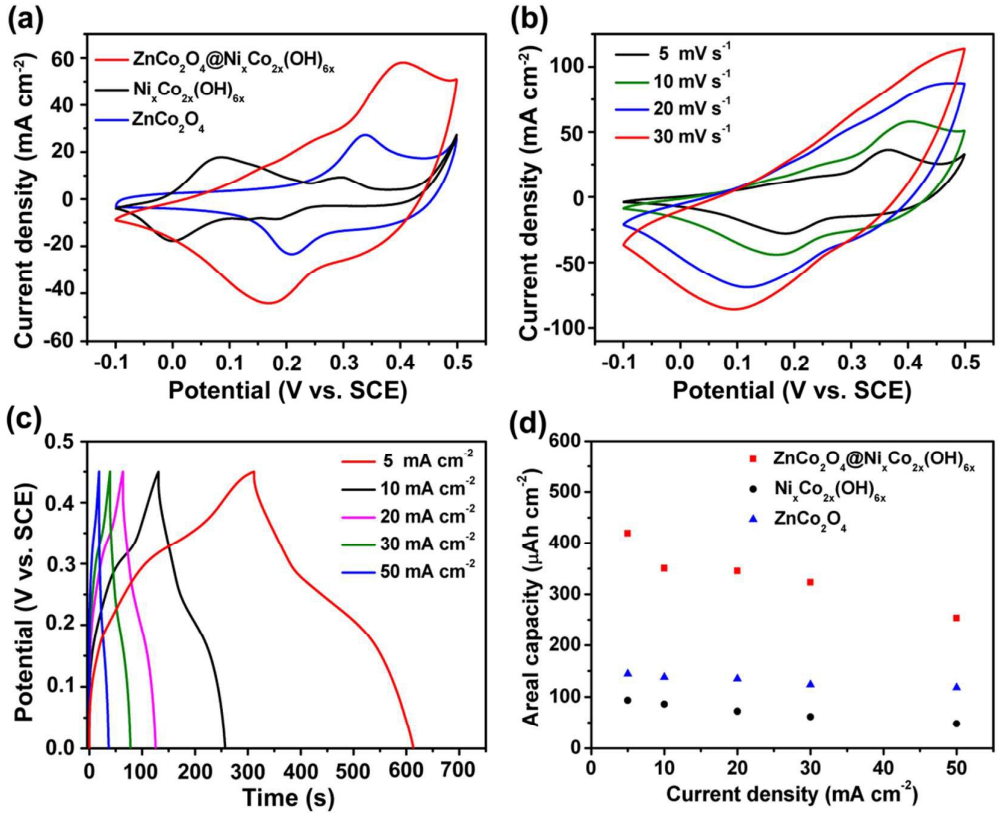

Fig. 6. (a) **A** comparison of CV curves for as-prepared $ZnCo_2O_4@Ni_xCo_{2x}(OH)_{6x}$, $Ni_xCo_{2x}(OH)_{6x}$ and $ZnCo_2O_4$ electrodes at a scan rate of 10 mV s^{-1}. (b) CV curves of the $ZnCo_2O_4@Ni_xCo_{2x}(OH)_{6x}$ electrode at different scan rates. (c) GCD curves of the $ZnCo_2O_4@Ni_xCo_{2x}(OH)_{6x}$ electrode at various current densities from 5 to 50 mA cm^{-2}. (d) The areal capacity as a function of current density for the $ZnCo_2O_4@Ni_xCo_{2x}(OH)_{6x}$, $Ni_xCo_{2x}(OH)_{6x}$ and $ZnCo_2O_4$ electrodes.

0.15 and 0.25 V can be seen in all curves and they reveal the battery-type characteristic of the hybrid electrode, which is consistent with the CV curves. Recently, Brousse *et al.* proposed that it would be most appropriate and meaningful to evaluate the capacity of battery-type electrodes and it would be essential to build a full device with a capacitive negative electrode.[8] The areal capacity of the electrodes can be calculated by the GCD curves (Fig. 6c and Fig. S5†) and equation (1). The mass loading of $Ni_xCo_{2x}(OH)_{6x}$ nanosheets coated on $ZnCo_2O_4$ nanowires can be controlled by varying the electrodeposition time. It is found that the hybrid electrode with the electrodeposition time of 10 min would have the highest areal capacity (Fig. S6†). The limited capacity of cleaned Ni foam is further confirmed by the GCD curves (Fig. S4b). As shown in Fig. 6d, the areal capacity of the optimized $ZnCo_2O_4@Ni_xCo_{2x}(OH)_{6x}$ electrode is up to 419.1 μAh cm^{-2} at 5 mA cm^{-2}, which is nearly 3 times as that of pristine $ZnCo_2O_4$ electrode (144.5 μAh cm^{-2}) and over 4 times as the value of the$Ni_xCo_{2x}(OH)_{6x}$ electrode (93.5 μAh cm^{-2}) at the same conditions. Such a high areal capacity is comparable to those of reported core/shell electrodes, such as $Co_3O_4@NiCo_2O_4$ (~ 311.7 μAh cm^{-2}),[49] $ZnO@Ni_3S_2$ (~ 318.5 μAh cm^{-2}),[50] $ZnCo_2O_4@Ni(OH)_2$ (~ 388.9 μAh cm^{-2})[24] and $NiCo_2S_4/Co_xNi_{1-x}(OH)_2$ (~ 397.2 μAh cm^{-2})[41]. Moreover, it can be found that the areal capacity gradually drops as the current density and there still remains 253.4 μAh cm^{-2} for the $ZnCo_2O_4@Ni_xCo_{2x}(OH)_{6x}$ electrode at a high current density of 50 mA cm^{-2} (60.6% retention of that at 5 mA cm^{-2}), demonstrating a good rate capability. These results highlight the advantages of the core/shell nanostructures.

Long-life cycling performance of the prepared electrodes was evaluated by repeated charge-discharge process at a current density of 20 mA cm^{-2} and the results are presented in Fig. 7a. For all the curves, the capacity retention slowly decreases with the cycle number. After 2000 cycles, the $Ni_xCo_{2x}(OH)_{6x}$ electrode retains only 53.8% of the initial capacity. While the retention of areal capacity for the $ZnCo_2O_4$ electrode is as high as 85.6%, exhibiting good cycling stability. With the rational combination of $ZnCo_2O_4$ nanowires and $Ni_xCo_{2x}(OH)_{6x}$ nanosheets, the overall retention for the hybrid electrode is still 81.4% after 2000 cycles, which is much better than the $Ni_xCo_{2x}(OH)_{6x}$ electrode and verifies its superiority as an advanced electrode. Electrochemical impedance spectroscopy (EIS) was carried out to investigate the electrical conductivity and ion diffusion. The corresponding Nyquist plots (Fig. 7b) can be fitted with an equivalent circuit (inset of Fig. 7b). At low frequency, the slope of the curve demonstrates the Warburg resistance (*W*), representing the electrolyte diffusion into the electrode. It is found that the *W* values of all the three electrodes are almost same. At high frequency, the intersection

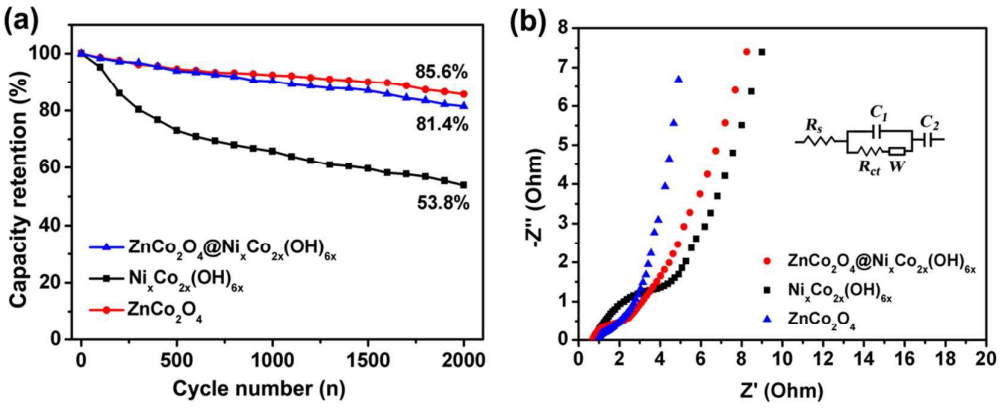

Fig. 7 (a) Cycling performance of the prepared $ZnCo_2O_4@Ni_xCo_{2x}(OH)_{6x}$, $Ni_xCo_{2x}(OH)_{6x}$ and $ZnCo_2O_4$ electrodes during 2000 cycles at 20 mA cm^{-2}. (b) Nyquist plots of $ZnCo_2O_4@Ni_xCo_{2x}(OH)_{6x}$, $Ni_xCo_{2x}(OH)_{6x}$ and $ZnCo_2O_4$ electrodes.

point on the real axis shows bulk resistance (R_s) of the electrochemical system and a higher R_s value indicates a lower electrical conductivity of the sample and vice versa. The semicircle displays the charge-transfer resistance (R_{ct}) which results from the Faradaic reactions and the double-layer capacitance on the electrode surface.[6,36,51] The fitted values of R_s, R_{ct} and W for the three electrodes are listed in Table S1†. Impressively, the $ZnCo_2O_4@Ni_xCo_{2x}(OH)_{6x}$ electrode exhibits a lower bulk resistance (0.75 Ω) and charge-transfer resistance (1.12 Ω) than those of the $Ni_xCo_{2x}(OH)_{6x}$ electrode (0.82 Ω and 2.02 Ω, respectively), which is owning to the good conductivity of the $ZnCo_2O_4$ nanowires. The hybrid electrode displays a little higher charge transfer resistance than pristine $ZnCo_2O_4$ electrode. It is due to the influence from the low conductivity of the $Ni_xCo_{2x}(OH)_{6x}$ nanosheet shell. Furthermore, the Bode plots (Fig. S7†) reveal that the hybrid electrode can show slower response time than that of the $Ni_xCo_{2x}(OH)_{6x}$ electrode.

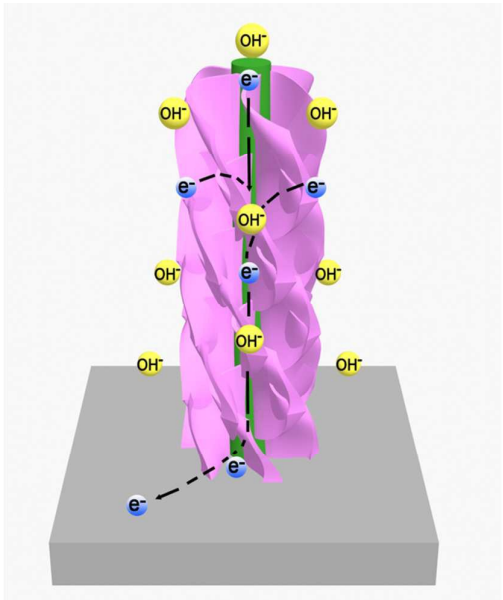

Fig. 8 Schematic illustration of the advantages of the hierarchical $ZnCo_2O_4@Ni_xCo_{2x}(OH)_{6x}$ NWAs

As expected, the $ZnCo_2O_4@Ni_xCo_{2x}(OH)_{6x}$ electrode shows high areal capacity, good rate capability and cycling stability, which mainly benefits from the core/shell structures and the synergetic effect between each component. Fig. 8 illustrates the advantages of the hierarchical $ZnCo_2O_4@Ni_xCo_{2x}(OH)_{6x}$ NWAs Firstly, the $ZnCo_2O_4$ NWAs, tightly attaching on the surface of conductive Ni foam and serving as backbones, can create a porous and stable 3D network. This conductive network would facilitate electrolyte ion diffusion and electron transport during the reversible electrochemical reactions. The interconnected $Ni_xCo_{2x}(OH)_{6x}$ nanosheets, coated on the $ZnCo_2O_4$ NWA backbones, are ultrathin and porous, which can provide larger surface area and more active sites. Finally, the rational construction can make the best of the each component resulting in a synergetic effect. These inherent advantages are expectable to make the hierarchical $ZnCo_2O_4@Ni_xCo_{2x}(OH)_{6x}$ core/shell NWAs particularly attractive.

To further evaluate the practical performance of the $ZnCo_2O_4@Ni_xCo_{2x}(OH)_{6x}$ NWAs, we have fabricated a hybrid supercapacitor with the hierarchical core/shell NWAs as the positive electrode, AC as the negative electrode and a piece of cellulose paper as the separator, as illustrated in Fig. 9a. The electrochemical performance of the device can be optimized by balancing the charges stored in the positive (Q_+) and negative (Q_-) electrodes. To obtain $Q_+ = Q_-$, the charge can be balanced based on the following equation:

$$\frac{A_+}{m_-} = \frac{C_{s-}\Delta V_-}{Q_{a+}} \quad (8)$$

where A_+ is the area and Q_{a+} is the areal capacity of the $ZnCo_2O_4@Ni_xCo_{2x}(OH)_{6x}$ electrode; m_- is the mass, C_{s-} is the specific capacitance and ΔV_- is the potential range of AC. We have investigated the capacitive performance of AC in the three-electrode system by CV and GCD measurements and the results are shown in Fig. S8†. It is found that the AC can present a specific capacitance of 180.7 F g^{-1} at a current density of 5 mA cm^{-2} with a potential window of -1.2−0 V. Due to the $ZnCo_2O_4@Ni_xCo_{2x}(OH)_{6x}$ electrode has a size of ~ 1 cm^2, the

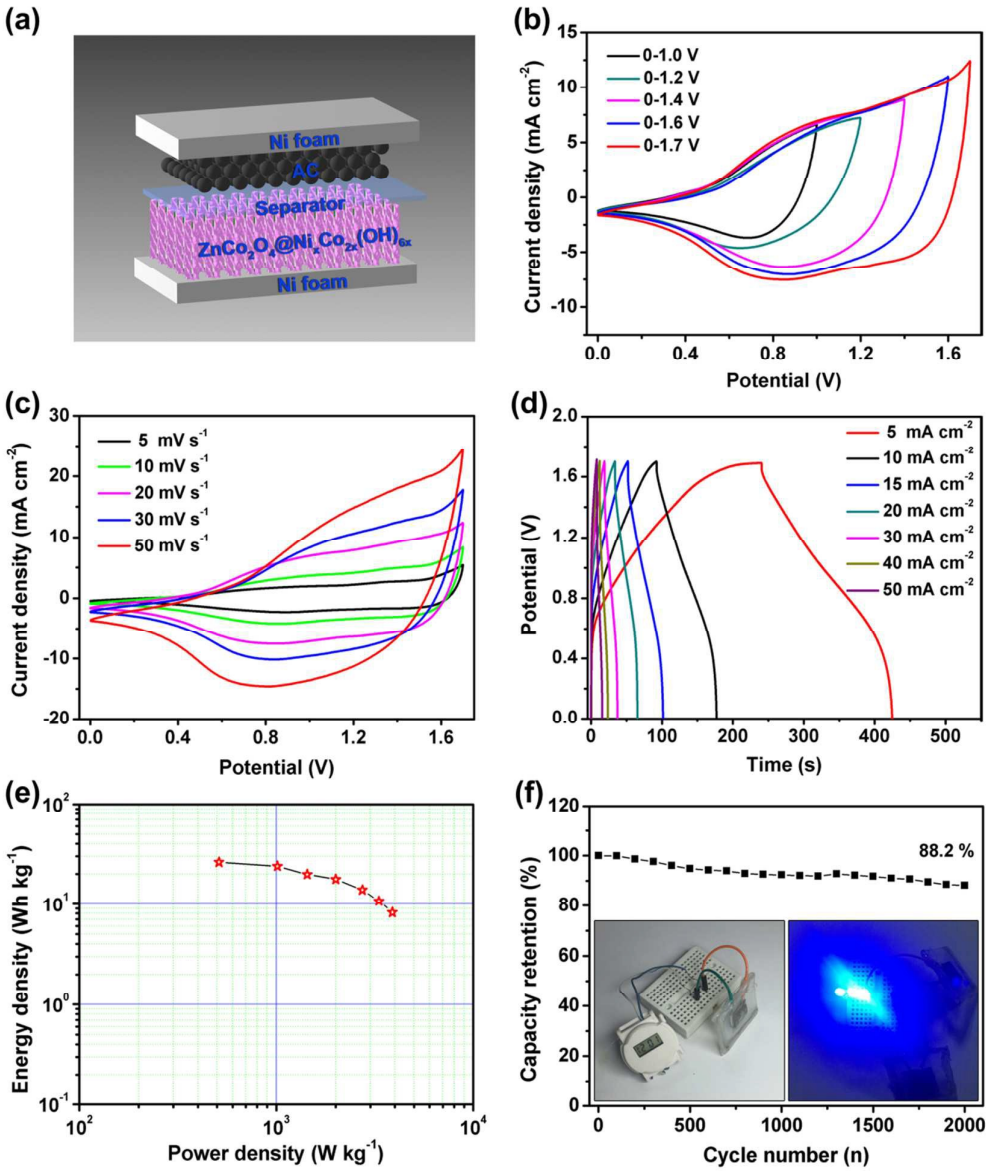

Fig. 9 (a) Schematic illustration of the assembled hybrid supercapacitor. (b) CV curves of the hybrid device within different voltage windows at a scan rate of 20 mV s^{-1}. (c) CV curves of the device with various scan rates (5−50 mV s^{-1}). (d) GCD curves of the device at different current densities (5−50 mA cm^{-2}). (e) Ragone plot of the hybrid device. (f) Cycling stability of the device for 2000 cycles at a constant current density of 30 mA cm^{-2}.

mass of AC should be balanced as ~ 6.96 mg. In the prepared hybrid device, the real mass of AC is ~ 7.0 mg and thus the total mass loading of active materials is about 9.5 mg. The operation potential window can be extended from -0.1 to 0.5 V for the $ZnCo_2O_4@Ni_xCo_{2x}(OH)_{6x}$ electrode and -1.2−0 V for the AC electrode in 2 M KOH electrolyte, according to their CV curves at 20 mV s^{-1} (Fig. S9†). The CV curves of the fabricated $ZnCo_2O_4@Ni_xCo_{2x}(OH)_{6x}$//AC hybrid supercapacitor within different voltage windows at the scan rate of 20 mV s^{-1} are shown in Fig. 9b. It can be found that the hybrid device can operate under a large voltage window of 0−1.7 V. When increasing the scan rates, the CV profiles (Fig. 9c†) can be well persevered, suggesting a high-rate capability. GCD curves of the hybrid device are shown in Fig. 9d. Based on the GCD curves and equation (3) and (4), the hybrid supercapacitor presents an areal energy density of 2.49 Wh m^{-2} at a power density of 48.6 Wh m^{-2}, as shown in Fig. S10†. Rogone plot of the device is shown in Fig. 9e. Though the high mass loading of active materials, the hybrid device can deliver a maximum energy density of 26.2 Wh kg^{-1} at 511.8 W kg^{-1}. This high energy density of our device is better than those of some reported hybrid supercapacitor such as $Co_3O_4@MnO_2$//AC (17.7 Wh kg^{-1})[33], Ni@Ni(OH)$_2$//AC (21.8 Wh kg^{-1})[18] and $NiCo_2O_4@NiCo_2O_4$//AC (15.42 Wh kg^{-1})[52]. It is also found that

the hybrid device presents a good cycling stability. Even at a high current density of 30 mA cm^{-2}, its capacity retention is as high as 88.2% after 2000 cycles (Fig. 9f). In addition, the assembled $ZnCo_2O_4@Ni_xCo_{2x}(OH)_{6x}$//AC hybrid device can easy power an electronic watch (~ 1.5V) after charging for 33 s and two charged hybrid devices in series can light 3 blue LED indicators (5 mm, 20 mA), as demonstrated in the inset of Fig. 9f. These results further signify the superiority of our $ZnCo_2O_4@Ni_xCo_{2x}(OH)_{6x}$ core/shell NWAs.

4. Conclusions

In summary, hierarchical $ZnCo_2O_4@Ni_xCo_{2x}(OH)_{6x}$ core/shell NWAs have been successfully designed and synthesized combining a hydrothermal method and an electrodeposition process. The $ZnCo_2O_4$ NWAs exhibit a good conductivity and stability, serving as backbones. Interconnected $Ni_xCo_{2x}(OH)_{6x}$ nanosheets were subsequently electrodeposited on the nanowire backbones, forming unique hierarchical core/shell nanowire arrays. The core/shell NWAs can make use of the hierarchical structures and the synergetic effect between each component. The novel electrode based on the core/shell structures exhibited a high areal capacity of 419.1 μAh cm^{-2}, as well as good rate capability and cycle performance. We have assembled a hybrid supercapacitor using the $ZnCo_2O_4@Ni_xCo_{2x}(OH)_{6x}$ NWAs as the positive electrode and AC as the negative electrode. The hybrid device can show a high energy density of 26.2 Wh kg^{-1} at a power density of 511.8 W kg^{-1}, revealing that the hierarchical $ZnCo_2O_4@Ni_xCo_{2x}(OH)_{6x}$ NWAs have great potential for applications in hybrid supercapacitors and this effective strategy also casts a new light on the design and synthesis of core/shell hybrid nanostructures for energy storage devices.

Acknowledgements

This work was financially supported by the National Natural Science Foundation of China (Grant No. 61176058 and 61404066).

References

1 A. S. Arico, P. Bruce, B. Scrosati, J.-M. Tarascon and W. van Schalkwijk, *Nat. Mater.*, 2005, **4**, 366-377.
2 C. Liu, F. Li, L. P. Ma and H. M. Cheng, *Adv. Mater.*, 2010, **22**, 28-62.
3 Q. Zhang, E. Uchaker, S. L. Candelaria and G. Cao, *Chem. Soc. Rev.*, 2013, **42**, 3127-3171.
4 X. Peng, L. Peng, C. Wu and Y. Xie, *Chem. Soc. Rev.*, 2014, **43**, 3303-3323.
5 G. Wang, L. Zhang and J. Zhang, *Chem. Soc. Rev.*, 2012, **41**, 797-828.
6 J. Chang, M. Jin, F. Yao, T. H. Kim, V. T. Le, H. Yue, F. Gunes, B. Li, A. Ghosh, S. Xie and Y. H. Lee, *Adv. Funct. Mater.*, 2013, **23**, 5074-5083.
7 F. Zhang, T. Zhang, X. Yang, L. Zhang, K. Leng, Y. Huang and Y. Chen, *Energy Environ. Sci.*, 2013, **6**, 1623-1632.
8 T. Brousse, D. Belanger and J. W. Long, *J. Electrochem. Soc.*, 2015, **162**, A5185-A5189.
9 D. P. Dubal, O. Ayyad, V. Ruiz and P. Gomez-Romero, *Chem. Soc. Rev.*, 2015, **44**, 1777-1790.
10 Q. Ke, M. Zheng, H. Liu, C. Guan, L. Mao and J. Wang, *Sci. Rep.*, 2015, **5**, 13940.
11 J.-K. Chang, C.-M. Wu and I. W. Sun, *J. Mater. Chem.*, 2010, **20**, 3729-3735.
12 X. Li, S. Xiong, J. Li, J. Bai and Y. Qian, *J. Mater. Chem.*, 2012, **22**, 14276-14283.
13 M. Yu, W. Wang, C. Li, T. Zhai, X. Lu and Y. Tong, *NPG Asia Mater.*, 2014, **6**, e129.
14 W. Fu, C. Zhao, W. Han, Y. Liu, H. Zhao, Y. Ma and E. Xie, *J. Mater. Chem. A*, 2015, **3**, 10492-10497.
15 H. Wang, H. S. Casalongue, Y. Liang and H. Dai, *J. Am. Chem. Soc.*, 2010, **132**, 7472-7477.
16 B. G. Choi, M. Yang, S. C. Jung, K. G. Lee, J.-G. Kim, H. Park, T. J. Park, S. B. Lee, Y.-K. Han and Y. S. Huh, *ACS Nano*, 2013, **7**, 2453-2460.
17 J. Ji, L. L. Zhang, H. Ji, Y. Li, X. Zhao, X. Bai, X. Fan, F. Zhang and R. S. Ruoff, *ACS Nano*, 2013, **7**, 6237-6243.
18 Y.-Z. Su, K. Xiao, N. Li, Z.-Q. Liu and S.-Z. Qiao, *J. Mater. Chem. A*, 2014, **2**, 13845-13853.
19 J. Li, M. Yang, J. Wei and Z. Zhou, *Nanoscale*, 2012, **4**, 4498-4503.
20 C. Shang, S. Dong, S. Wang, D. Xiao, P. Han, X. Wang, L. Gu and G. Cui, *ACS Nano*, 2013, **7**, 5430-5436.
21 L. Qu, Y. Zhao, A. M. Khan, C. Han, K. M. Hercule, M. Yan, X. Liu, W. Chen, D. Wang, Z. Cai, W. Xu, K. Zhao, X. Zheng and L. Mai, *Nano Lett.*, 2015, **15**, 2037-2044.
22 H. Chen, Q. Zhang, J. Wang, Q. Wang, X. Zhou, X. Li, Y. Yang and K. Zhang, *Nano Energy*, 2014, **10**, 245-258.
23 T. W. Kim, M. A. Woo, M. Regis and K.-S. Choi, *J. Phys. Chem. Lett.*, 2014, **5**, 2370-2374.
24 H. X. Chuo, H. Gao, Q. Yang, N. Zhang, W. B. Bu and X. T. Zhang, *J. Mater. Chem. A*, 2014, **2**, 20462-20469.
25 Y. Sharma, N. Sharma, G. V. Subba Rao and B. V. R. Chowdari, *Adv. Funct. Mater.*, 2007, **17**, 2855-2861.
26 Y. Qiu, S. Yang, H. Deng, L. Jin and W. Li, *J. Mater. Chem.*, 2010, **20**, 4439-4444.
27 B. Liu, B. Liu, Q. Wang, X. Wang, Q. Xiang, D. Chen and G. Shen, *ACS Appl. Mater. Interfaces*, 2013, **5**, 10011-10017.
28 S. Wang, J. Pu, Y. Tong, Y. Cheng, Y. Gao and Z. Wang, *J. Mater. Chem. A*, 2014, **2**, 5434-5440.
29 G. Zhou, J. Zhu, Y. Chen, L. Mei, X. Duan, G. Zhang, L. Chen, T. Wang and B. Lu, *Electrochim. Acta*, 2014, **123**, 450-455.
30 W. Fu, X. Li, C. Zhao, Y. Liu, P. Zhang, J. Zhou, X. Pan and E. Xie, *Mater. Lett.*, 2015, **149**, 1-4.
31 I. K. Moon and K.-Y. Chun, *RSC Adv.*, 2015, **5**, 807-811.
32 Z. Sun, W. Ai, J. Liu, X. Qi, Y. Wang, J. Zhu, H. Zhang and T. Yu, *Nanoscale*, 2014, **6**, 6563-6568.
33 M. Huang, Y. Zhang, F. Li, L. Zhang, Z. Wen and Q. Liu, *J. Power Sources*, 2014, **252**, 98-106.
34 W. Ma, H. Nan, Z. Gu, B. Geng and X. Zhang, *J. Mater. Chem. A*, 2015, **3**, 5442-5448.
35 X. Xia, J. Tu, Y. Zhang, J. Chen, X. Wang, C. Gu, C. Guan, J. Luo and H. J. Fan, *Chem. Mater.*, 2012, **24**, 3793-3799.
36 D. Cai, B. Liu, D. Wang, L. Wang, Y. Liu, H. Li, Y. Wang, Q. Li and T. Wang, *J. Mater. Chem. A*, 2014, **2**, 4954-4460.
37 W. Yang, Z. Gao, J. Ma, X. Zhang, J. Wang and J. Liu, *J. Mater. Chem. A*, 2014, **2**, 1448-1457.
38 J. Wang, D. Chao, J. Liu, L. Li, L. Lai, J. Lin and Z. Shen, *Nano Energy*, 2014, **7**, 151-160.
39 J. Zhu, L. Huang, Y. Xiao, L. Shen, Q. Chen and W. Shi, *Nanoscale*, 2014, **6**, 6772-6781.
40 L. Yu, G. Zhang, C. Yuan and X. W. Lou, *Chem. Commun.*, 2013, **49**, 137-139.

41 J. Xiao, L. Wan, S. Yang, F. Xiao and S. Wang, *Nano Lett.*, 2014, **14**, 831-838.
42 L. Huang, D. Chen, Y. Ding, Z. L. Wang, Z. Zeng and M. Liu, *ACS Appl. Mater. Interfaces*, 2013, **5**, 11159-11162.
43 L. Huang, D. Chen, Y. Ding, S. Feng, Z. L. Wang and M. Liu, *Nano Lett.*, 2013, **13**, 3135-3139.
44 W. Luo, X. Hu, Y. Sun and Y. Huang, *J. Mater. Chem.*, 2012, **22**, 8916-8921.
45 T. F. Hung, S. G. Mohamed, C. C. Shen, Y. Q. Tsai, W. S. Chang and R. S. Liu, *Nanoscale*, 2013, **5**, 12115-12119.
46 U. M. Patil, M. S. Nam, J. S. Sohn, S. B. Kulkarni, R. Shin, S. Kang, S. Lee, J. H. Kim and S. C. Jun, *J. Mater. Chem. A*, 2014, **2**, 19075-19083.
47 L. Hu, B. Qu, C. Li, Y. Chen, L. Mei, D. Lei, L. Chen, Q. Li and T. Wang, *J. Mater. Chem. A*, 2013, **1**, 5596-5602.
48 X. Liu, S. Shi, Q. Xiong, L. Li, Y. Zhang, H. Tang, C. Gu, X. Wang and J. Tu, *ACS Appl. Mater. Interfaces*, 2013, **5**, 8790-8795.
49 G. Zhang, T. Wang, X. Yu, H. Zhang, H. Duan and B. Lu, *Nano Energy*, 2013, **2**, 586-594.
50 Z. Xing, Q. Chu, X. Ren, C. Ge, A. H. Qusti, A. M. Asiri, A. O. Al-Youbi and X. Sun, *J. Power Sources*, 2014, **245**, 463-467.
51 C.-W. Huang and H. Teng, *J. Electrochem. Soc.*, 2008, **155**, A739-A744.
52 X.-F. Lu, D.-J. Wu, R.-Z. Li, Q. Li, S.-H. Ye, Y.-X. Tong and G.-R. Li, *J. Mater. Chem. A*, 2014, **2**, 4706-4713.

A table of contents entry

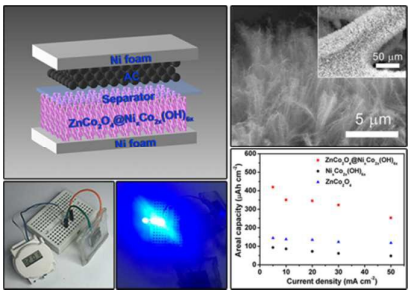

Hierarchical $ZnCo_2O_4$@$Ni_xCo_{2x}(OH)_{6x}$ core/shell nanowire arrays have been successfully constructed for hybrid supercapacitors with outstanding performance.